ChemComm
Chemical Communications

Accepted Manuscript

This article can be cited before page numbers have been issued, to do this please use: J. De, A. H. M. M., R. A. K. Yadav, S. P. Gupta, I. Bala, P. Chawla, K. Kishore Kesavan, J. Jou and S. K. Pal, *Chem. Commun.*, 2020, DOI: 10.1039/D0CC05813K.

ROYAL SOCIETY OF CHEMISTRY

rsc.li/chemcomm

View Article Online
DOI: 10.1039/D0CC05813K

COMMUNICATION

AIE-Active Mechanoluminescent Discotic Liquid Crystals for Applications in OLEDs and Bio-Imaging

Received 00th January 20xx,
Accepted 00th January 20xx

DOI: 10.1039/x0xx00000x

Joydip De,[a] Abdul Haseeb M. M.,[a] Rohit Ashok Kumar Yadav,[b] Santosh Prasad Gupta,[c] Indu Bala,[a] Prateek Chawla,[d] Kiran Kishore Kesavan,[b] Jwo-Huei Jou,[b] and Santanu Kumar Pal*[a]

A multifunctional molecular design of fluorescent discotic liquid crystal (DLC) consisting of tetraphenylethylene core is reported which is found to serve as an excellent solid-state emitter in OLED devices with EQE of 4.4% and tunable mechanochromism. X-ray diffraction studies unveiled that change in supramolecular self-assembly is the physical origin of mechanochromism. The luminescent DLC molecule has been shown to act as a highly selective probe for labelling acidic cellular compartments (such as lysosomes) in bio-imaging using HeLa cells.

Construction of fascinating columnar supramolecular architecture formed by molecular self-assembly has drawn incredible attention in recent years due to its various intriguing applications.[1] However, the field remains challenging in terms of designing new functional materials for superior optical applications,[2] especially in bio-imaging and organic light-emitting devices. Hereof, liquid crystals (LC) that form columnar phases can lead to dynamic soft materials,[3] the properties of which can be tuned to meet the aforesaid desired applications. Most traditional columnar phases formed by discotic liquid crystals (DLCs) show strong luminescence in dilute solutions; however, they experience poor emission at concentrated solutions or in the solid-state due to strong π-π interactions of the cores[4] leading to the formation of excimers or exciplexes[5] (aggegation caused quenching, ACQ). Nevertheless, this phenomena curbed their rampant applications in most solid-state emitting devices. In contrast, aggregation-induced emission (AIE) active luminogen, first discovered by Tang et al.[6] uncovers a new area[7] in which molecules show high emission in the aggregated state can act as a potential alternative in solid-state devices. Certainly, it is in acute demand and challenging

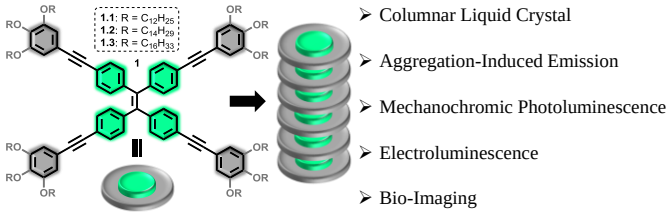

Scheme 1. Design of multi-functional columnar DLCs.

task to obtain materials that render the chasm between these two phenomena (AIE vs ACQ) that will add benefit for cutting-edge applications. Herein, we have developed a new approach to a design of tetraphenylethylene (TPE) based luminescent columnar discotics (Scheme 1) for advanced applications such as bio-imaging and highly efficient organic light-emitting diodes (OLEDs) employing them as solid-state emitters. Cell imaging of HeLa cells demonstrated the utility of TPE discotic as a novel probe for labelling acidic cellular compartments such as lysosomes with good stability. In OLED devices, maximum brightness of 1768 cd m^{-2} with the emitter **1.1** having an external quantum efficiency of 4.4% has been perceived. The columnar assembly of DLCs facilitates the faster movement of charge carrier[1d,8a,8b], prerequisite to efficient recombination process in OLEDs. In addition, these DLC materials can serve as potent mechano-responsive luminogens.

Detailed synthesis and characterizations of the compounds (**1.1-1.3**) are discussed in Scheme S1 and Figure S1-S6. All the compounds were found to exhibit high thermal stability as observed from their thermogravimetric analysis (TGA) (Figure S7) data. In differential scanning calorimetry (DSC), all the materials during heating and cooling scan exhibited a single peak that corresponds to mesophase to isotropic transition and *vice versa*. For example, compound **1.1** displayed isotropization at 52.1 °C (with heat of transition Δ*H* of 12.43 $kJmol^{-1}$) and a peak at 43.2 °C (Δ*H* = 9.30 $kJmol^{-1}$), on cooling from the isotropic liquid. All the compounds show similar behaviour in DSC, as mentioned in details in ESI (Table S1, Figure S8). In all cases, under polarizing optical microscopy (POM), the appearance of a well-defined texture (Figure 1a,

[a] Department of Chemical Sciences,[d]Department of Biological Sciences, Indian Institute of Science Education and Research (IISER) Mohali, Knowledge city, Sector 81, SAS Nagar, Manauli 140306, India. E-mail: skpal@iisermohali.ac.in; santanupal.20@gmail.com
[b] Department of Materials Science and Engineering, National Tsing Hua University, Hsinchu 30013, Taiwan.
[c] Department of Physics, Patna University, Patna-800005, India.
Electronic Supplementary Information (ESI) available: See DOI: 10.1039/x0xx00000x

1b, Figure S9) was observed which remained stable down to room temperature (even down to -40 °C). The mesophases of **1.2** and **1.3** were deduced as columnar hexagonal (Col_h) on the basis of typical textures observed by POM and of their X-ray diffraction experiments. However, for **1.1**, the obtained X-ray pattern is consistent with the columnar oblique (Col_{ob}) phase (see below).

To deduce the exact nature of the mesophase assembly small and wide angle X-ray Scattering (SAXS/WAXS) experiments have been performed. The SAXS/WAXS pattern of **1.1** at temperature 25 °C is shown in Figure 1c. It exhibits many narrow peaks in small-angle region, whereas, in the wide-angle regime, it shows one broad peak (h_a) and one weak peak (h_c). The wide-angle peak, h_a (*d*-spacing of ~4.84 Å) is typical of liquid-like order of the aliphatic chains, and h_c (*d*-spacing of ~3.53 Å) is indicative of π-π interaction of the cores. In small angle, the diffraction pattern could be indexed on an oblique lattice with lattice parameters *a* = 58.38 Å, *b* = 43.65 Å and angle α = 40.42° (Figure 1c, Table S2). Thus, the assembly is Col_{ob} in the mesophase of **1.1.** The SAXS/WAXS pattern of **1.2** at 25 °C exhibits many narrow peaks in small-angle region with *d*-spacing in ratio $1: 1/\sqrt{3}: 1/\sqrt{7}: 1/\sqrt{13}$ and correspond to reflection from the planes (10), (11), (21), and (31), of hexagonal lattices, respectively, with lattice parameter *a* = 45.34 Å (Figure 1d , Table S3). Further, in wide-angle region, one narrow peak (h_{ac}) with d-spacing 4.50 Å, appears due to partially crystallized alkyl chain and there is also a backgroud (h_a), originated mainly due to the correlations of fluid chains. Moreover, h_c peak with *d*-spacing of ~3.53 Å (indicative of π-π interaction) is observed in the wide angle region. Overall, the structure remains Col_h in the mesophase of **1.2**. Similar to **1.2**, compound **1.3** exhibited Col_h nature in its mesophase (Figure S10, Table S4) as inferred from SAXS/WAXS analysis.

Further, to have a better understanding of the arrangement of molecules in their respective phases, electron density map

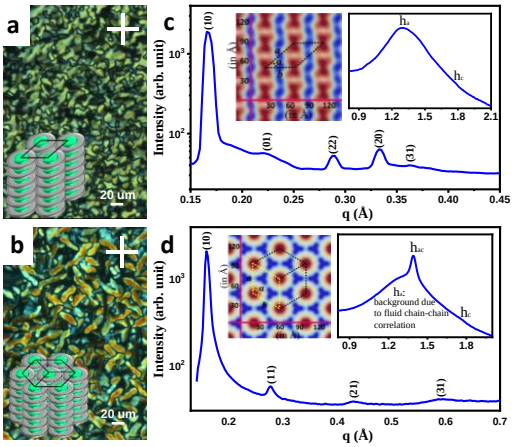

Figure 1. POM image of (a) **1.1** at 26.2 °C and (b) **1.2** at 25.7 °C under crossed polarizers on cooling. SAXS/WAXS pattern of (c) **1.1** in Col_{ob} and (d) **1.2** in Col_h mesophase at 25°C. Inset of (c) and (d) shows EDM of **1.1** in Col_{ob} and **1.2** in Col_h mesophase, respectively. Deep red and blue represents the highest and lowest electron density, respectively.

(EDM)[8] has been constructed by using the information of the peaks indexes and intensities. The EDM for the compounds **1.1-1.3** (Figure 1c (inset), 1d (inset) and S11) represents the clear visualization of nano segregated columnar assembly in their respective mesophases.

In order to study the photophysical behaviour of compound **1.1-1.3**, UV-vis and photoluminescence (PL) spectroscopy were performed in solution (10^{-6} M in THF) and solid-state. In solution, compound **1.1** showed three absorption peaks having peak maxima (λ_{max}) at 330 nm and only one emission peak at 534 nm (Figure S12a). On the contrary, it showed two absorption peaks with maxima at 337 nm and one emission peak at 505 nm in solid-state (Figure S13a). Compound **1.2** and **1.3** exhibited similar kind of absorption and emission behaviour as represented in Figure S12-S13. Interestingly, TPE-derivatives**,** exhibited the aggregation-induced emission (AIE) phenomena, with yellow-green colour emission. To study the AIE behaviour different fraction of water (in increasing order) was added into the solution of material **1.1** in THF (Figure 2a and S14).[9] It is observed that at 0 % water fraction (f_w) it exhibits emission with significantly less intensity. With increasing f_w up to 20%, the emission intensity remains the same. After that, it increased upon adding more amount f_w at 30%-70%. Then at 90 % f_w maximum emission was observed (Figure S14a-S14b). Compound **1.2** and **1.3** also exhibited similar AIE behaviour as observed in Figure S15. To gain more insight into the luminescence efficacy, fluorescence quantum yield was measured for all the TPE derivatives (**1.1-1.3**) and found to be 76.89%, 72.91% and 70.18% for **1.1**, **1.2** and **1.3**, respectively in the technologically important solid-state.

Excitingly, compound **1.1** is sensitive to external stimuli and exhibited tunable mechanochromic fluorescence property. The compound showed yellowish-green colour, which upon grinding changed to cyan colour as observed under 365 nm UV light (Figure 2b inset). The PL peak is hypsochromically shifted from 505 nm to 487 nm upon grinding (Figure 2b). While after fumed in dichloromethane (DCM), the ground film recovered its original luminescence, i.e. it exhibits reversible

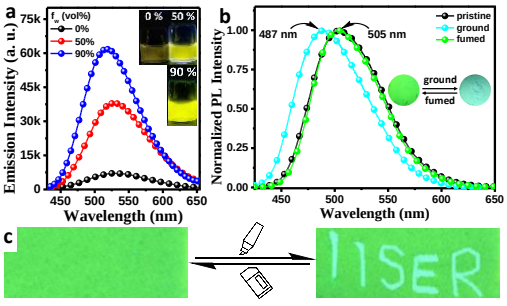

Figure 2. (a) PL spectra of **1.1** with different water fractions, f_w (vol %). Inset represents the images of the solutions of **1.1** with different f_w under 365 nm UV light. (b) PL spectra of **1.1** before and after grinding, also after exposing it to DCM vapour. λ_{ex} = 330 nm. Inset shows the corresponding images of **1.1** with different conditions under UV light. (c) Image of writing and erasing of letter "IISER" on a filter paper by using **1.1**, under UV light.

mechanochromism. In addition, Figure S16 represents the repeated switching of the mechanochromic luminescence behaviour of compound **1.1** upon mechanical grinding and subsequently fumed with DCM for five cycles. Similarly,

compound **1.2** and **1.3** also exhibited mechanochromic behaviour (Figure S17). In order to study the physical origin of the mechanochromism, X-ray diffraction (XRD) measurement of **1.1-1.3** was performed in the film state before (pristine) and after grinding. From Figure S18 and Table S4-S10, it is clear that changes in molecular self-assembly upon grinding i.e. from Col_{ob} to Col_h for **1.1** and Col_h to Col_r for **1.2** and **1.3** is responsible for mechanochromism.[10] Moreover, the electron density maps derived from the XRD patterns of **1.2** obtained before and after grinding provided clear visualization of the change in their assembly as shown in the Figure S19. This mechanochromic PL behaviour is further studied for practical application such as rewritable paper. In order to do so, a filter paper is immersed in the DCM solution of **1.1**. After drying, it showed yellowish-green colour, on which the word "IISER" was written by glass rod, and it appeared in cyan colour under 365 nm UV light (Figure 2c). After exposing this filter paper in DCM for a few minutes, the appearance of the written letter "IISER" vanished. Thus, compound **1.1** can be potentially applicable to security inks.

To get an insight about the electrochemical behaviour of **1.1-1.3**, cyclic voltammetry (CV) has been carried out. In the CV spectra (Figure S20), all the derivatives (**1.1-1.3**) exhibit similar oxidation and reduction behaviour. The HOMO/LUMO values are -5.53 eV/-3.39 eV, -5.48 eV/-3.43 eV and -5.50 eV/-3.38 eV, for **1.1**, **1.2** and **1.3,** respectively (Table S11). The DFT calculations of **1.1-1.3** were performed to observe the molecular geometry and electronic delocalization in their corresponding frontier molecular orbitals. It is observed that both the HOMO and LUMO are mainly localized over the central TPE core with little contribution from peripheral alkynyl benzene units (Figure S21). In such kind of systems, the charge transport is expected to be high, due to an increased overlap among the frontier molecular orbitals of the discotic cores[11], which will lead to the better performance in devices.

The excellent photophysical and thermal characteristics of the TPE based DLC molecules inspired us to study its suitability as potential electroluminescent materials. For this, solution-processed OLED devices have been fabricated with the configuration of ITO/ PEDOT:PSS (35 nm)/ CBP: x wt% emitter(x = 1.0, 3.0, 5.0, and 100) (25nm)/ TPBi (40 nm)/ LiF (1.5 nm)/ Al (150 nm) using compound **1.1-1.3** as emitter (Figure S22a). The OLED devices exhibited bright blueish-green emission (λ_{max} = 500-508 nm) in electroluminescence (EL) spectra for emitters (Figure 22b inset) and their corresponding CIE coordinates are provided in Figure S22b. The current density- voltage-luminance (I-V-L) and current efficiency-luminance-power efficiency characteristics of the devices are illustrated in Figure 3a-3b, and pertinent data are summarized in Table 1 and Table S12. It is observed that OLED device fabricated with compound **1.1** (3.0 wt%) exhibited the best performance among all of the studied devices (Figure S23-S25, Table S12). The EQE-luminance plots of the devices are displayed in Figure S26. The device performance shown by the columnar TPE mesogens (as emitter) displays

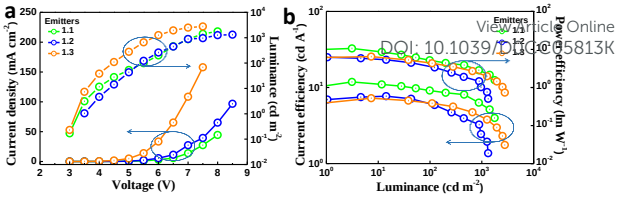

Figure 3. (a) Current density-voltage-luminescence and (b) current efficiency-luminance-power efficiency plots of OLEDs consist of 3 wt% emitters (**1.1-1.3**) doped in CBP host.

Table 1. Electroluminescence behaviour of **1.1-1.3**

Emitter	Turn-on Voltage (V)	$PE_{max}/CE_{max}/EQE_{max}$ [a] ($lmW^{-1}/cdA^{-1}/\%$)	CIE Coordinates [b]	Max. Lum. ($cd\ m^{-2}$)
1.1	3.1	10.6/11.8/4.4	(0.23,0.44)	1768
1.2	3.5	6.2/7.7/3.4	(0.23,0.41)	1324
1.3	3.1	6.5/7.2/2.7	(0.22,0.43)	2777

[a] Maximum power efficiency (PE), current efficiency (CE), and EQE. [b]CIE coordinates at 100 cd m^{-2}.

favourable balance between two complementary characteristics, i.e. luminescent and charge transport which can be further revealed by the low turn-on voltages of the device (Table 1). To analyze the charge transport in the OLED devices, hole-only device (HOD) and electron-only device (EOD) have been fabricated. The current density-voltage (J-V) characteristics of the HOD, EOD, and reference device (CBP:**1.1** 3.0 wt%) are displays in Figure S27. The reference device exhibits high current density at a low voltage compared to the HOD and EOD, which indicates better injection of charge carriers from the respective electrodes and favourable charge transport across the layers for the recombination process[12], hence better device performance. In addition, the photoluminescence quantum yield (PLQY, Φ_{PL}) measurements of the best emitter (i.e. **1.1**) doped at different concentrations (1.0, 3.0 and 5.0 wt%) into CBP host demonstrates that the emitter **1.1** with 3.0 wt% exhibited a PLQY of 81.75% and achieves a maximum EQE of 4.4% (Table S12 and S13). This fact suggests that the PLQY of the system (host:guest) is one of a key parameter that possesses a significant contribution in evaluating the EQEs of the devices.[13] Further, atomic force microscopy (AFM) measurement of the films of **1.1**:CBP with different doping concentrations (1.0, 3.0 and 5.0 wt%) (Figure S28) was performed and the films exhibited uniform surface morphology with no observable cracks or pinholes with very low surface roughness which is a prerequisite to achieve efficient OLEDs. The EL spectra of the devices closely resemble corresponding PL spectra (thin-film state) of the emitters (Figure S29), suggesting that the EL emission arises from the intrinsic emission and excited states of the emitters.

The interesting fluorescence pattern displayed by the present DLCs prompted us to assess their application in cellular imaging. To test the efficacy of the compound as a potential fluorophore, HeLa cells were incubated with varying concentrations of **1.1**. Based on the expression pattern, 7.5 µM was selected as a suitable concentration for further

experiments (representative image Figure 4a). Investigating the cells using confocal laser

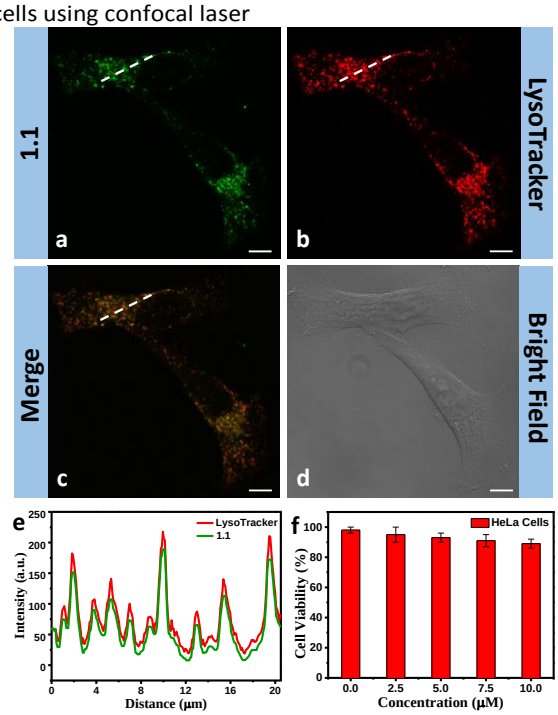

Figure 4. CLSM image of HeLa cells stained with (a) **1.1**, (b) LysoTracker Red DND-99, (c) co-localization of **1.1** with LysoTracker Red DND-99 and (d) bright field image. Scale bar = 10 μm. (e) Intensity profile of the region of interest (represented with dashed line). (f) Cytotoxicity assay.

scanning microscopy (CLSM) revealed that **1.1** undergoes excitation at 488 nm, giving a bright green emission pattern. Additionally, to elucidate its subcellular localisation, we co-incubated HeLa cells with **1.1** and LysoTracker Red DND-99, a fluorescent acidotropic probe for labelling acidic organelles in live cells. Interestingly, we observed that **1.1** co-localises with LysoTracker dye (Figure 4b-4d), as depicted in the intensity profile pattern (Figure 4e). Furthermore, to investigate the cytotoxicity of the compound, we performed cell viability measurements using a quantitative and sensitive MTT cell assay kit. HeLa cells were incubated with varying concentrations (0 to 10 μM) of **1.1,** and the results suggested negligible toxicity to HeLa cells, thereby highlighting its bio-compatibility. Given its high stability, negligible cytotoxicity and precise subcellular localisation, the compound displays an immense potential as a novel probe for labelling acidic cellular compartments (such as lysosomes).[14]

In conclusion, a new design of TPE based columnar DLC was shown to act as a highly efficient emitter in OLEDs with a maximum EQE of 4.4% and beholds an immense potential to serve as a probe for selective labelling of cellular compartments such as lysosomes. The present strategy unveils a new horizon for the development of multi-functional DLC smart materials.

SKP, JD and IB acknowledge Project File No. CRG/2019/000901/OC, (09/947(0220)/2019/EMR-I) and (02(0311)/17/EMR-II), respectively. We thank central as well as departmental facilities and confocal facility (ZEISS LSM710) at IISER Mohali.

Conflicts of interest

View Article Online
DOI: 10.1039/D0CC05813K

"There are no conflicts to declare".

References

1 (a) T. Kato, M. Yoshio, T. Ichikawa, B. Soberats, H. Ohno and M. Funahashi, *Nat. Rev.*, 2017, **2**, 17001; (b) L. Schmidt-Mende, A. Fechtenkötter, K. Müllen, E. Moons, R. H. Friend and J. D. MacKenzie, *Science*, 2001, **293**, 1119; (c) S. Xiao, M. Myers, Q. Miao, S. Sanaur, K. Pang, M. L. Steigerwald and C. Nuckolls, *Angew. Chem. Int. Ed.*, 2005, **44**, 7390; (d) C. Ruiz, E. M. G. Frutos, G. Hennrich and B. G. Lor, *J. Phys. Chem. Lett.*, 2012, **3**, 1428; (e) T. Wöhrle, I. Wurzbach, J. Kirres, A. Kostidou, N. Kapernaum, J. Litterscheidt, J. C. Haenle, P. Staffeld, A. Baro, F. Giesselmann and S. Laschat, *Chem. Rev.*, 2016, **116**, 1139.

2 (a) H.-T. Feng, Y.-X. Yuan, J.-B. Xiong, Y.-S. Zheng and B. Z. Tang, *Chem. Soc. Rev.*, 2018, **47**, 7452; (b) H. Qu, Y. Wang, Z. Li, X. Wang, H. Fang, Z. Tian and X. Cao, *J. Am. Chem. Soc.*, 2017, **139**, 18142.

3 (a) S. Kumar, *Chem. Soc. Rev.*, 2006, **35**, 83; (b) C. T. Imrie and P. A. Henderson, *Chem. Soc. Rev.*, 2007, **36**, 2096 (c) C. Tschierske, *Angew. Chem. Int. Ed.*, 2013, **52**, 8828; (d) T. Kato, J. Uchida, T. Ichikawa and T. Sakamoto, *Angew. Chem. Int. Ed.*, 2018, **57**, 4355.

4 (a) S. Moyano, J. Barbera, B. E. Diosdado, J. L. Serrano, A. Elduque and R. J. Gimenez, *J. Mater. Chem. C*, 2013, **1**, 3119; (b) B. Zhang, C.-H. Hsu, Z.-Q. Yu, S. Yang and E.-Q. Chen, *Chem. Commun.*, 2013, **49**, 8872: (c) R. Gimenez, M. Pinol and J. L. Serrano, *Chem. Mater.*, 2004, 16, 1377.

5 J. B. Birks, Wiley-Interscience: London, 1970.

6 J. D. Luo, Z. L. Xie, J. W. Y. Lam, L. Cheng, H. Y. Chen, C. F. Qiu, H. S. Kwok, X. W. Zhan, Y. Q. Liu, D. B. Zhu and B. Z. Tang, *Chem. Commun.*, 2001, 1740.

7 (a) J. Mei, N. L. Leung, R. T. Kwok, J. W. Lam and B. Z. Tang, *Chem. Rev.*, 2015, **115**, 11718; (b) Z. Zhao, H. Zhang, J. W. Lam and B. Z. Tang, *Angew. Chem. Int. Ed.*, 2020, **59**, 9888.

8 (a) J. De, I. Bala, S. P. Gupta, U. K. Pandey and S. K. Pal, *J. Am. Chem. Soc.*, 2019, **141**, 18799; (b) I. Bala, J. De, S. P. Gupta, H. Singh, U. K. Pandey and S. K. Pal, *Chem. Commun.*, 2020, **56**, 5629.

9 (a) S. Jiang, J. Qiu, Y. Chen, H. Guo and F. Yang, *Dyes. Pigm.*, 2018, **159**, 533; (b) H. Jing, L. Lu, Y. Feng, J. F. Zheng, L. Deng, E. Q. Chen and X. K. Ren, *J. Phys. Chem. C*, 2016, **120**, 27577.

10 (a) Y. Sagara and T. Kato, *Nature Chem.*, 2009, **1**, 605; (b) Y. Sagara, S. Yamane, M. Mitani, C. Weder and T. Kato, *Adv. Mater.* 2016, **28**, 1073; (c) S. Yamane, Y. Sagara, T. Mutai, K. Araki and T. Kato, *J. Mater. Chem. C*, 2013, **1**, 2648.

11 S. J. Mahoney, M. M. Ahmida, H. Kayal, N. Fox, Y. Shimizu and S. H. Eichhorn, *J. Mater. Chem.*, 2009, **19**, 9221.

12 (a) X. Zhang, C. Fuentes-Hernandez, Y. Zhang, M. W. Cooper, S. Barlow, S. R. Marder and B. Kippelen, *J. Appl. Phys.*, 2018, **124**, 055501; (b) P. Juhasz, J. Nevrela, M. Micjan, M. Novota, J. Uhrik, L. Stuchlikova, J. Jakabovic, L. Harmatha and M. Weis, *Beilstein J. Nanotechnol.*, 2016, **7**, 47.

13 (a) Z. Xu, B. Z. Tang, Y. Wang and D. Ma, *J. Mater. Chem. C*, 2020, **8**, 2614; (b) T. Miwa, S. Kubo, K. Shizu, T. Komino, C. Adachi and H. Kaji, *Sci. Rep.*, 2017, **7**, 284.

14 (a) X. Zheng, W. Zhu, D. Liu, H. Ai, Y. Huang and Z. Lu, *ACS Appl. Mater. Interfaces*, 2014, **6**, 7996; (b) X. Zheng, W. Zhu, F. Ni, H. Ai, S. Gong, X. Zhou, J. L. Sessler and C. Yang, *Chem. Sci.*, 2019, **10**, 2342.

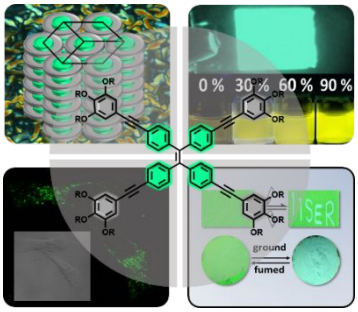

View Article Online
DOI: 10.1039/D0CC05813K

A multifunctional molecular design of fluorescent discotic liquid crystal consisting of tetraphenylethylene core is reported for OLEDs, mechanochromism and bio-imaging applications.